

Rapid sliding and friction degradation: Lessons from the catastrophic Vajont landslide



Juan Pablo Ibañez^{a,*}, Yossef H. Hatzor^b

^a Department of Civil Engineering, National University of Cuyo, Mendoza, Argentina

^b Department of Geological and Environmental Sciences, Ben-Gurion University of the Negev, Beer-Sheva, Israel

ARTICLE INFO

Keywords:

Friction degradation
Rapid shear
Vajont landslide
DDA

ABSTRACT

We use the numerical, discrete element, Discontinuous Deformation Analysis (DDA) method to study velocity - distance evolution of the catastrophic Vajont landslide using a newly implemented friction degradation law based on empirical evidence that peak friction is mobilized in rock discontinuities after displacement distance of $\approx 1\%$ of overriding block length.

It has been established by previous researchers that during the catastrophic event the slide moved across a basal plane that possessed a friction angle of 12° only ($\mu = 0.231$) due to previous sliding events. When the catastrophic event was triggered, most likely due to excessive filling of the reservoir, friction had to be further degraded to explain the mapped runout distance and the estimated duration of the event. We find that further friction degradation of 25% must have taken place both across the basal plane as well as in the rock joints consisting the sliding mass. This degradation resulted in 25 m/s peak velocity of the sliding mass, about 570 m runout distance, and sliding duration of 37 s.

Our back-analyzed friction - velocity relationship expands the range of velocity and displacement values that can be controlled experimentally using rotary shear tests, by an order of magnitude. With the aid of numerical analysis, therefore, catastrophic landslides can become natural experiments at the field scale that provide ultimate friction degradation values for clay filled rock discontinuities. Using the case of the Vajont landslide we find that frictional resistance across clay-filled dolomite interfaces cannot degrade to values lower than $\mu = 0.16$.

1. Introduction

The Vajont landslide (sometimes spelled “Vaiont”) occurred on 9 October 1963 in a slope near the Vajont dam, north of Italy. A mass of approximately 300 million m^3 of rock and debris collapsed into the reservoir generating a wave that over-topped the 261.6 m high dam. The wave-generated flood filled the valley destroying the town of Longarone downstream, and other villages nearby. More than 2000 people were killed. Hendron and Patton (1985) estimated that the Vajont landslide moved a 250 m thick mass of rock over 400 to 500 m horizontally until the sliding mass was stopped at the opposite side of the valley wall. They estimated 20 to 25 m/s peak velocities, and a maximum of 45 s of motion. After more than 50 years, the Vajont landslide is still considered one of the most catastrophic slope failures in recent times and an outstanding case history for the study and back analysis of complex instability mechanisms associated with deep-seated landslides (Barla and Paronuzzi, 2013).

Fig. 1 shows one transverse section before and after the catastrophic

landslide of October 1963. It has been established that the landslide was a reactivation of an old landslide, and that it was triggered by fluctuations in the reservoir level (Hendron and Patton, 1987). The landslide occurred over a detachment surface developed across clay-filled dolomites. The sliding surface is shown in Fig. 2 and a detail of the clay-filled basal plane is shown in Fig. 3.

An extensive body of research was published on the Vajont landslide over the past five decades. Most noted are the technical report by Giudici and Semenza (1960) from at the time of dam construction, the studies of Prof. Muller on the failure mechanisms (Müller, 1964, 1968), and the expert report by Hendron and Patton (1985) that provides comprehensive description and analysis of the case. Nowadays, more than hundred scientific papers and technical reports are available (Superchi et al., 2010). Recent research is typically focused on new field investigations, collecting new and interpreting available data about the case history, and developing geological, analogue and numerical modeling approaches in order to better explain the main characteristics of the slide (e.g. Tika and Hutchinson, 1999; Semenza and Ghirotti,

* Corresponding author.

E-mail addresses: jpibanez@fing.uncu.edu.ar (J.P. Ibañez), hatzor@bgu.ac.il (Y.H. Hatzor).

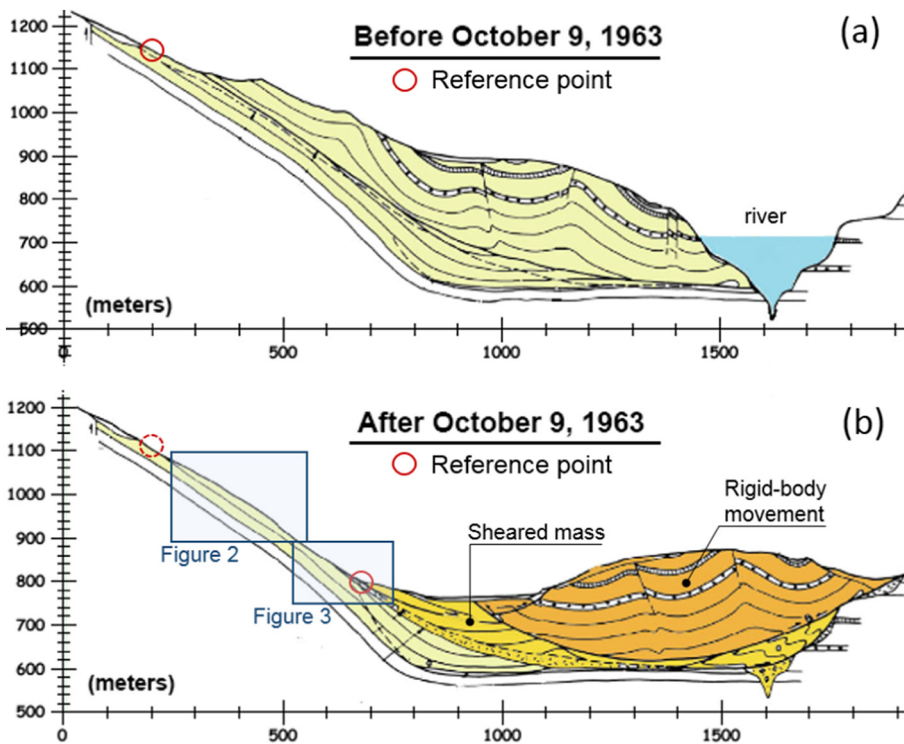


Fig. 1. Cross section through the Vajont slide before (a) and after (b) the October 1963 event (modified after Hendron and Patton, 1985). The reference point used for velocity estimation is shown as red circle. Location of photos shown in Figs. 2 and 3 are shown in in blues boxes. (For interpretation of the references to color in this figure legend, the reader is referred to the web version of this article.)



Fig. 2. General view of the scarp of the Vajont slide.



Fig. 3. Detail of the dolomite basal plane of the Vajont slide.

2000; Semenza, 2001; Alonso and Pinyol, 2010; Pinyol and Alonso, 2010; Paronuzzi and Bolla, 2015; Wolter et al., 2016) and to probe deeper into possible shear heating mechanisms (e.g. Veveakis et al., 2007; Goren and Aharonov, 2009).

Although the Vajont landslide has been the subject of numerous studies, some questions still remain unresolved, especially regarding the causes of the failure, the origin of the extreme velocities, and the influence of reservoir level (Del Ventisette et al., 2015).

The onset of sliding has been related to sudden breakage of marly-calcareous rock bridges across the basal sliding plane (Nonveiller, 1986; Hutchinson, 1988; Hutchinson, 1987). From a mechanical point of view, the main issue that must be clarified is the very high value of the estimated velocities. Two main hypotheses have been proposed:

- Excessive, heat generated, pore pressure across the sliding surface (e.g. Romero and Molina, 1974; Habib, 1975; Voight and Faust, 1982; Hendron and Patton, 1985; Nonveiller, 1986; Vardoulakis, 2000; Goren and Aharonov, 2007);
- Low dynamic friction of the clayey interbeds across the sliding surface (e.g. Tika and Hutchinson, 1999).

Temperature increase along a low permeability and high plasticity basal surface could have triggered pore pressure increase leading to 25 m/s peak velocity, according to limit equilibrium analysis performed by Hendron and Patton (1985). Some argue, however, that this alone would be insufficient to explain the dynamics of the Vajont landslide (Alonso and Pinyol, 2010; Pinyol and Alonso, 2010).

The numerical, discrete element, discontinuous deformation analysis (DDA) method (Shi, 1993; Hatzor et al., 2017) was used to study the Vajont slide by Sitar et al. (2005) who have focused primarily on the kinematics of the failure process. By comparing the velocity time histories of different measurement points in the DDA model of the sliding mass, they concluded that the mass moved coherently along the basal plane. They further found that peak velocity increased by up to 50% with increasing number of blocks in the DDA model (from 12 through 28 to 105 in different models), suggesting that internal disintegration of the sliding mass prompted increased slide accelerations. They have

implemented shear strength reduction in DDA based on the Voight and Faust (1982) model for pore pressure generation due to shear heating, and obtained this way velocity time histories close to the results obtained by Hendron and Patton (1985). Wang et al. (2013) proposed a trilinear friction law and a cohesion cut-off to model the Vajont landslide with DDA, however their model consisted of only 9 blocks and no attempt to analyze the velocity time history was made.

In this paper we study the velocity evolution of the Vajont slide with DDA using very detailed block model based on accurate field maps and cross sections. For better understanding of the block size effect, we compare 10 models consisting of 176, 388, 805, 1421, 2149, 2578, 3079, 3775, 4764 and 6255 blocks. We implement friction degradation across the joints as a function of displacement in DDA and obtain velocity time histories. The results of our numerical analyses with DDA confirm the analytical results obtained by Hendron and Patton (1985) with respect to the velocity time history of the slide and the runout distance. Furthermore, we believe our numerical results constrain the ultimate friction degradation that can be expected during rapid shearing across clay-filled weakness planes in geological materials such as dolomites.

2. Friction degradation during sliding

2.1. Shear strength of initially rough discontinuities

Patton (1966) proposed a bilinear criterion for shear strength of initially rough rock surfaces:

$$\tau = \sigma_n \tan(\phi_b + i) \quad (1)$$

where σ_n is normal stress, " ϕ_b " is the basic friction of a perfectly smooth interface which is typically equal to the residual friction angle of sheared interface, and " i " is the roughness angle. Undoubtedly, the roughness degrades during shear (Rengers, 1970). Recently the issue of roughness evolution through shear has been explored in some detail using profile measurements with laser scanning technology coupled with servo-controlled direct shear testing. Results clearly show that roughness degrades with sliding distance (Davidesko et al., 2014) whereas the influence of normal stress on roughness evolution is more complicated (Badt et al., 2016).

Scale affects both the peak shear strength of the interface, as well as the shear distance necessary to reach it (Barton, 1973; Barton and Bandis, 1980; Bandis et al., 1981). From the experimental results published by Barton and Choubey (1977) it appears that a displacement of approximately 1% of the overriding block length would be necessary to mobilize peak frictional resistance when shearing pre-existing, initially rough, discontinuities. We use this empirical observation in the development of our proposed bi-linear friction degradation model for DDA.

2.2. Proposed friction law for DDA

Several enhanced friction laws have recently been implemented in DDA for improving the shear behavior in forward modeling (Mizoguchi et al., 2007; Bakun-Mazor et al., 2012; Huang et al., 2016; Song et al., 2016; Ma et al., 2017; Togo et al., 2009).

We propose here a simple friction degradation law to allow more realistic dynamic sliding modeling with DDA. The main hypothesis is that as soon as sliding is initiated the roughness component begins to degrade due to shearing. This process continues until the roughness degrades completely and residual conditions are attained across the sliding surface; at that stage, frictional resistance is governed only by the residual friction angle ϕ_b (see Fig. 4). The input friction angle in the original DDA is assumed as peak friction ϕ_p . We include a known roughness angle value i for the joints which has to be introduced along with the peak friction angle value ϕ_p . In our modified DDA code we introduce a degradation parameter " D " that scales (from 0 to i) the

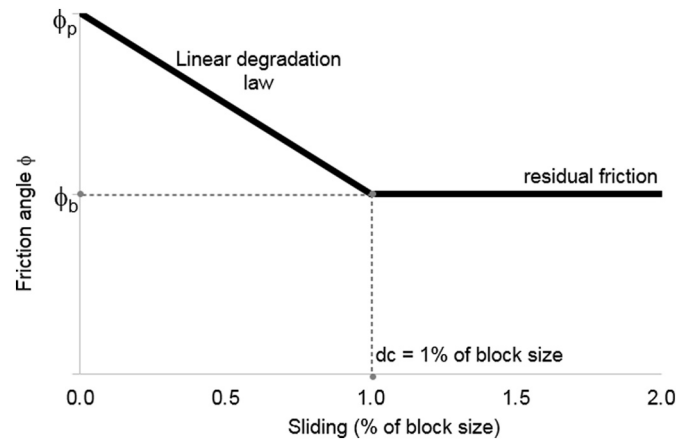


Fig. 4. Proposed bilinear friction law with degradation due to sliding.

amount of degradation that is applied on ϕ_p . We let D increase linearly with block displacement d . Maximum degradation ($D = i$) in every contact is reached when the amount of displacement equals 1% of the length of the overriding block at that contact, as per the empirical observations of Barton and Choubey (1977). We refer to that distance as the critical distance d_c , not to be confused with the state variable D_c of the rate and state friction theory (Dieterich, 1972; Ruina, 1983). When the displacement d is greater than d_c , the friction offered by the sliding surface is the residual or basic friction angle ϕ_b , and the degradation parameter D maintains its maximum value ($D = i$) throughout the sliding process, namely:

$$\begin{aligned} D &= i(d/d_c) \quad \text{if } (d < d_c) \\ D &= i \quad \text{if } (d \geq d_c) \end{aligned} \quad (2)$$

The dynamic friction angle during sliding is therefore (see Fig. 4):

$$\begin{aligned} \phi &= \phi_p - D \quad \text{if } (d < d_c) \\ \phi &= \phi_b = \phi_p - i \quad \text{if } (d \geq d_c) \end{aligned} \quad (3)$$

The implemented friction degradation model is applied to vertex-edge contacts in DDA. If for example the vertex belongs to block 1 and the edge belongs to block 2 then the degradation distance d_c is calculated as 1% of block 1 length. When displacement begins, the relative movement is stored in the vertex data of block 1. Based on the stored movement and the d_c value, the degradation D is calculated and the friction angle is updated accordingly. Finally, friction forces are calculated using the degraded friction value.

Note that this simple friction degradation model is purely mechanical and ignores other thermo-chemical processes such as shear heating, vaporization, and mineralization of the sliding surface. Note also that we ignore cohesion in the proposed law. Although cohesion degradation has been implemented, we chose to ignore it completely in the analysis, because as is typically the case with rock joints in general, the cohesion, if ever existed, is lost due to climatic effects and episodic displacements over time, and therefore is commonly ignored in dynamic DDA simulations.

2.3. Verification of the proposed friction law

The DDA method has been verified extensively for dynamic block motions using analytical solutions and laboratory tests (see Tsesarsky et al. (2005), Kamai and Hatzor (2008), Ning and Zhao (2012) and Yagoda Biran and Hatzor, 2016)). We use the classic problem of a block on an inclined plane (MacLaughlin et al., 2001) for validating the implementation of the proposed law (see Fig. 5). The inclination angle of the slope is α , and the friction angle of the sliding interface is ϕ . The forces acting on the block are its self-weight mg , the normal from the

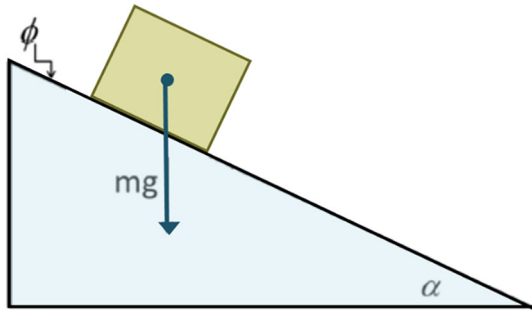


Fig. 5. Schematics of the block on an incline problem used for modified DDA validation.

plane N , and the frictional force at the interface between the block and the plane, $N \tan\phi$. Assuming constant friction, the downslope displacements of the block is:

$$d(t) = \frac{1}{2}g(\sin\alpha - \cos\alpha \cdot \tan\phi)t^2 + v_0t + d_0 \tag{4}$$

where g is gravity acceleration, v_0 is the initial block velocity, and d_0 is its initial displacement. Here the acceleration remains constant during sliding, given by

$$a = g(\sin\alpha - \cos\alpha \cdot \tan\phi)$$

For a bilinear friction law, the acceleration increases with the distance, and the acceleration term becomes:

$$a = g(\sin\alpha - \cos\alpha \cdot \tan(\phi_b + (1 - d/d_c) i)) \text{ if } (d < d_c) \tag{5}$$

$$a = g(\sin\alpha - \cos\alpha \cdot \tan(\phi_b)) \text{ if } (d \geq d_c)$$

DDA results for a 2:1 slope inclination ($\alpha = 26.6^\circ$) with constant friction of $\phi = 25^\circ$ and a $2.23 \text{ m} \times 2.05 \text{ m}$ size block are plotted in Fig. 6 along with the analytical solution (Eq. 4). The numerical error between DDA and the analytical solution is smaller than 0.5% throughout the simulation. Fig. 6 also shows the dynamic block displacements as computed with DDA for different initial roughness angles ($i = 1^\circ, 2^\circ, 5^\circ, 10^\circ$), using the proposed friction law. The block contact length is 2.23 m, and therefore “ d_c ” is 0.023 m. It can be appreciated that roughness degradation prompts increased sliding velocity which increases with decreasing residual friction value ($\phi_b = \phi - i$).

In order to verify the implementation of degradation, we compare the DDA acceleration response with the analytical solution provided by Eq. (5). We use the case of $\phi = 25^\circ$, $i = 5^\circ$ and “ d_c ” = 1%. The analytical acceleration is initially 0.296 m/s^2 , increasing up to a maximum value of 1.194 m/s^2 after which it remains constant. A very good agreement is obtained between both solutions as can be appreciated in

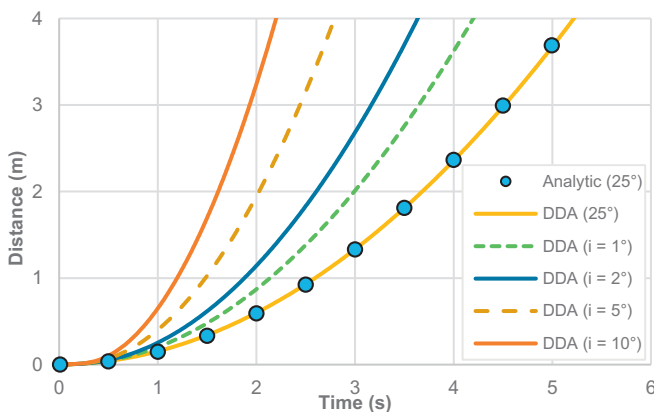


Fig. 6. Comparison between DDA and analytical solution for constant friction ($\phi = 25^\circ$). The effect of friction degradation on sliding evolution is also shown.

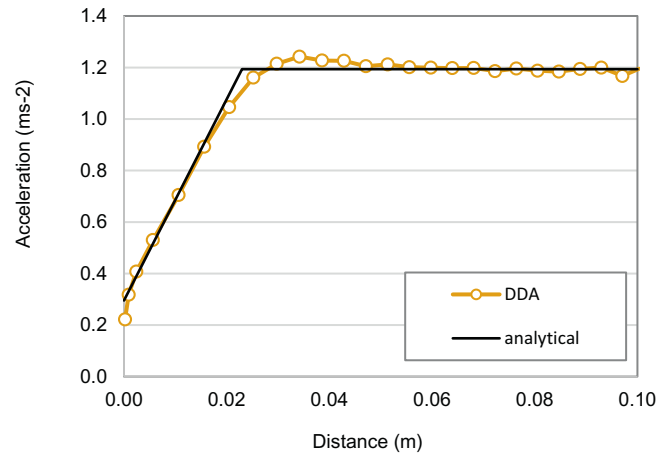


Fig. 7. Comparison of acceleration evolution as obtained with DDA and the analytical solution ($\phi = 25^\circ$, $i = 5^\circ$, $d_c = 1\%$).

Fig. 7; the relative error remaining less than 4% throughout the simulation.

3. The case of Vajont landslide

3.1. Shear strength

As discussed by Paronuzzi and Bolla (2015), the rock mass involved in the Vajont landslide suffered cumulative effects of damage processes. The well established paleo-slide degraded the original shear strength in both the basal plane as well as in the joints in the rock mass. Furthermore, it is assumed that some amount of healing occurred during the time span between the paleo landslide and the catastrophic event of 1963, a rapid sliding episode that triggered further damage processes within the sliding mass and across the basal plane.

From the early studies of the Vajont landslide (Müller, 1964; Lo et al., 1972; Chowdhury, 1978; Müller, 1968), the shear strength along the basal sliding plane was assumed to be governed by residual shear strength of the multiple clay layers present along the basal surface rather than the higher shear strength of rock-to-rock contacts. These assumptions were based primarily on field observations and laboratory shear tests, but also on Atterberg limit tests, borehole logs, and other geological evidence (Hendron and Patton, 1985, 1987).

It was assumed that essentially all peak strength components across the basal plane have been lost because of paleo slides. The residual strength of the clay layers in the basal plane, therefore, was assumed to be the most significant factor in the stability of the rock mass. It is reasonable to expect however time dependent strength increase across the basal plane, due to the presence of rock-to-rock contact areas, that over time could heal and offer resistance as rock bridges would within a rock joint surface (e.g. Eberhardt et al., 2004). During dam construction the slope was at limiting equilibrium, which was violated as the reservoir began to be filled. Water pressure at the basal plane triggered a progressive failure process that finally culminated in the catastrophic landslide.

Table 1 shows the friction values obtained by laboratory tests and

Table 1 Friction value for clay layer and rock mass (Hendron and Patton, 1985).

| Geological | Friction angle | | | Obs. |
|--------------|----------------|-----------------------|-------------------|----------------|
| Material | Symbol | Range of values | Recommended value | |
| Clay layer | α | $5^\circ - 16^\circ$ | 12° | Residual value |
| Rock mass | β | $30^\circ - 40^\circ$ | 40° | Peak value |
| Lateral mass | γ | $30^\circ - 40^\circ$ | 36° | Peak value |

the weighted values (considering residual values and healing influence) recommended by Hendron and Patton (1985) for stability analysis.

It was also clear from the earlier stability analyses that the rock mass could not have been stable with residual shear strength across the basal plane, and that an additional strengthening mechanism was necessary to achieve static stability. Three main possible strengthening mechanisms were suggested (Hendron and Patton, 1985):

- Lateral friction across the boundaries of the mobilized mass, in sub-vertical planes oriented parallel to the direction of the slide movement. The assumed friction value acting on the lateral boundaries was $\gamma = 36^\circ$ based on field observations and correlations with friction values in similar rocks.
- The basal sliding plane laterally dips a few degrees upstream, developing normal forces acting on vertical planes oriented parallel to the direction of the slide movements.
- In some parts of the slide the sliding surface did not develop along the clayey infilling planes but sheared across the bedded rocks, where healing process could have occurred;

Limit equilibrium analysis reveals that the sliding mass could not reach the estimated velocities and distances as described in the introduction, with the recommended shear strength values of Table 1. It was therefore necessary to find a feasible strength loss mechanism to explain the progressive failure. Several shear strength loss mechanisms have been proposed (Hendron and Patton, 1985):

- Displacement-induced reduction in β between rock mass blocks;
- Reduction from peak to residual shear strength along the part of the landslide where the sliding surface did not follow the bedding clayey planes but sheared across the bedding;
- Reduction in shear strength along the basal sliding plane in clay layers caused by heat-generated increase in pore pressure;

3.2. Estimated velocities

The main authoritative reference is the extensive geological-geotechnical report presented by Hendron and Patton (1985). In addition to many factual details involving the engineering geology of the site and the sequence of events that preceded the failure, three main conclusions can be obtained from Hendron and Patton's work with respect to the sliding mechanism:

- The slide lasted 45 s or less;
- The sliding mass moved horizontally about 400–500 m;
- The sliding mass reached velocities as high as 20–25 m/s;

In appendix E of Hendron and Patton's report an analysis of the landslide velocities using a static-dynamic limit equilibrium analysis is presented. The method applies a static stability analysis for estimating forces acting on the slide mass at any given position as the slide progresses downhill. The obtained forces are used to determine accelerations by dynamic calculation, and finally the velocities are obtained. For each step, the slide mass geometry is updated and a new static analysis is made. The β value is assumed as constant at 40° , and cohesion along the sliding interface is neglected. The static friction value ϕ_{static} in the sliding surface (α value) required for stability is then calculated. From this condition, an artificial degradation of the static friction value is applied in order to reproduce the dynamic condition for sliding with $\phi_{dynamic}$. The loss in strength is given by Hendron and Patton (1985) as follows:

$$\text{Friction loss (\%)} = \left[1 - \left(\frac{\phi_{dynamic}}{\phi_{static}} \right) \right] \cdot 100 \tag{6}$$

Degradation varying from 50 to 60% was set for obtaining

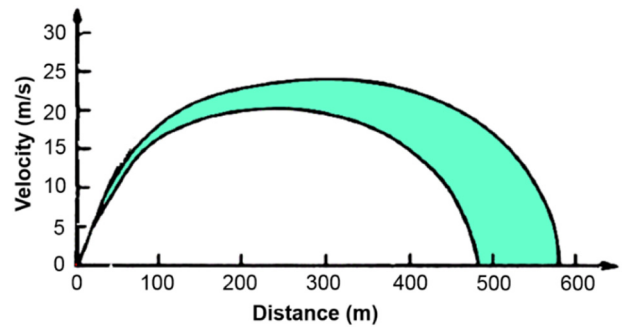


Fig. 8. Estimated lateral velocity/distance chart for friction loss varying from 50 to 60% as obtained analytically by Hendron and Patton (1985).

analytical velocity-distance curves that match field observations (see Fig. 8). The assumed friction loss is in fact a global concept that represents different effects that occur simultaneously in the deforming rock mass during sliding, including:

- Shear strength (α) degradation across the sliding interface. The total friction loss in the sliding interface was estimated by Hendron and Patton (1985) to be between 3° and 7° , from a nominal value of 12° , to 9° or 5° , respectively, due to peak to residual drop at several rock-to-rock contacts, and/or increase in water-pressure in the clayey material due to shear heating;
- Friction degradation in the rock mass joints (β). The total friction loss across the rock joints was estimated by Hendron and Patton (1985) to be 10° , dropping from 40° to 30° , due to relative block sliding between rock blocks that induced roughness degradation;
- Friction degradation across the lateral boundaries (γ). The total friction loss at the lateral boundaries was estimated by Hendron and Patton (1985) to be 11° , dropping from 36° to 25° , due to relative sliding that induced roughness degradation;

With these processes all acting simultaneously Hendron and Patton (1985) could explain the high velocities estimated for the Vajont slide.

3.3. DDA model

We use our proposed friction degradation model on geological cross section N° 5 in Hendron and Patton (1985) report (see Fig. 1a) to check the validity of their conclusions regarding the effects of friction degradation on slide velocity and distance, as discussed above. The rock mass involved in the slide extends 1400 m over a clay layer that constitutes the sliding surface (Fig. 9). The basal surface is sub horizontal at the valley (dip angle = 1.0°), and then the slope inclination progressively increases in the uphill direction (dip angle = $29\text{--}34^\circ$).

The numerical simulations are performed in two dimensions as the length of the sliding mass is much greater than its width and therefore a two-dimensional approximation is considered appropriate. Moreover, most of the friction degradation occurs in parallel to the sliding direction and not in the strike direction of the sliding plane, further limiting the advantage of adopting a full three dimensional approach. Although as mentioned above some lateral shear resistance is offered by the boundaries of the sliding mass, modeling this in three dimensions would severely limit the total number of blocks in the sliding mass that could be handled in the dynamic simulations without seriously compromising solution accuracy.

Based on geological profiles proposed by Müller (1964, 1968) and Paronuzzi and Bolla (2015) the rock mass is represented in DDA by three principal joint sets: vertically dipping joints, gently dipping bedding-plane, and sub horizontal joints parallel to the basal surface. That joint set configuration reproduces a masonry-type fabric, as observed in field. The boundary condition is given by the fixed basal

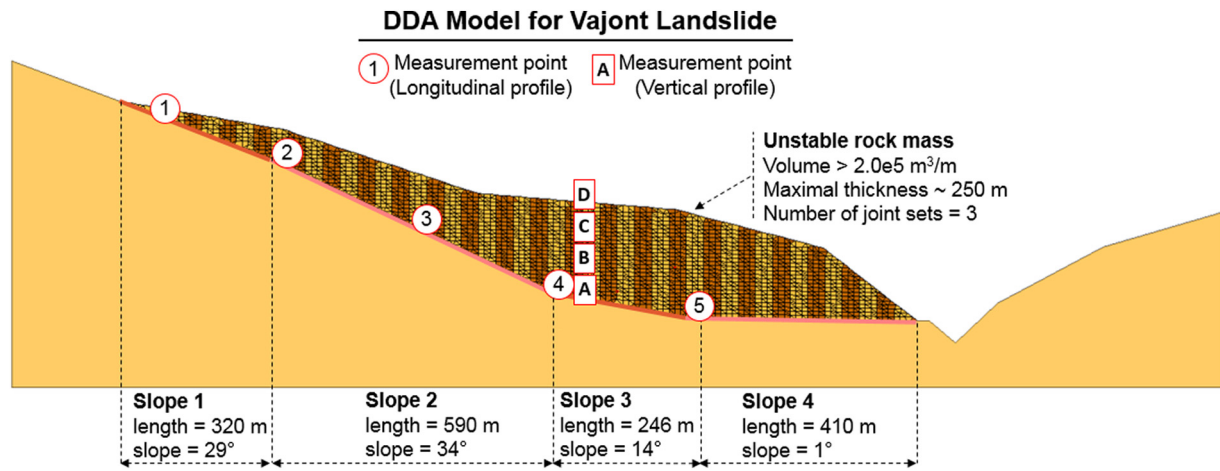


Fig. 9. DDA model of section N° 5 (Fig. 1a) showing longitudinal and vertical profiles of measurement points.

Table 2

DDA sections used for reproducing the structure of the Vajont landslide.

| DDA Section | Number of blocks | Block size (average) meters |
|-------------|------------------|-----------------------------|
| I | 176 | 34.3 |
| II | 388 | 23.1 |
| III | 805 | 16.0 |
| IV | 1421 | 12.1 |
| V | 2149 | 9.8 |
| VI | 2578 | 8.9 |
| VII | 3079 | 8.2 |
| VIII | 3775 | 7.4 |
| IX | 4764 | 6.6 |
| X | 6255 | 5.7 |

block. Therefore, fixed points are distributed along the basal plane. Time increment and contact stiffness are automatically updated between time steps in the DDA version we use in this research (Shi, 2010). The value of the contact stiffness (or the penalty) is computed such that the maximum penetration at all closed contact positions are less than a given limit. The chosen stiffness value represents non-linear contact spring: it is small for small contact force and large for large contact force.

We simulate 10 DDA sections to analyze the effect of block size on displacement and velocity as detailed in Table 2. Section VII, that fits well the reported 5–20 m fracture pattern, is the chosen reference section for DDA simulations.

3.4. DDA simulations

Hendron and Patton (1985) recommended friction values are shown in Table 1. They suggested $\beta = 40^\circ$ for all the joints in the rock mass and $\alpha = 12^\circ$ for the sliding surface (clay layer). These parameters are adopted here as reference (peak) friction parameters for all DDA simulations.

a) Reference state

First we performed DDA simulations on section VII using the reference parameters mentioned above with no degradation. Under these conditions we obtained runout distance of 292 m, peak velocity of 11.9 m/s and a duration of 40.0 s. Clearly friction degradation is necessary to match the back analyzed parameters reported by Hendron and Patton (1985).

b) Stable state

Next we wanted to find the required parameters for static stability. We found that in order to obtain a stable state in section VII, a friction angle across the basal plane of 22° is required. This value should be

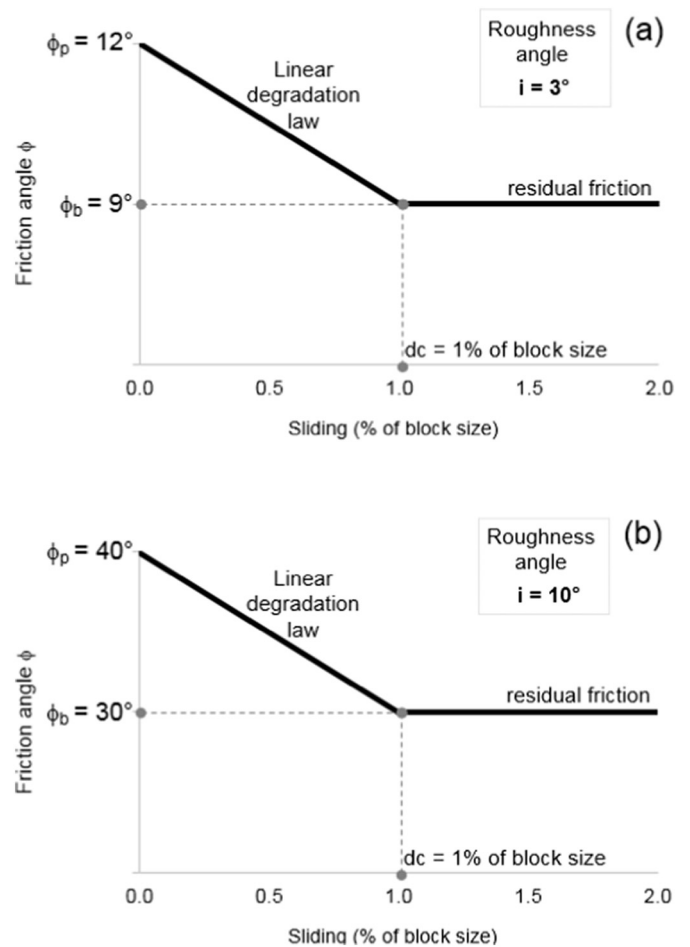


Fig. 10. Bilinear friction model with degradation for a) clay layer; b) rock mass.

considered as a lower boundary of the peak friction angle value that was available across the basal plane before any motion took place in the geological history of the cross section. It has been established (Giudici and Semenza, 1960; Müller, 1964; Hendron and Patton, 1985) that the catastrophic failure in Vajont was in fact a rejuvenation of an old landslide. Therefore, it is reasonable to assume that before the catastrophic event residual friction values prevailed across the basal plane. With residual friction conditions across the basal plane we must assume that the slide was kept in place before the catastrophic event by virtue of one of the temporary strengthening mechanisms discussed above.

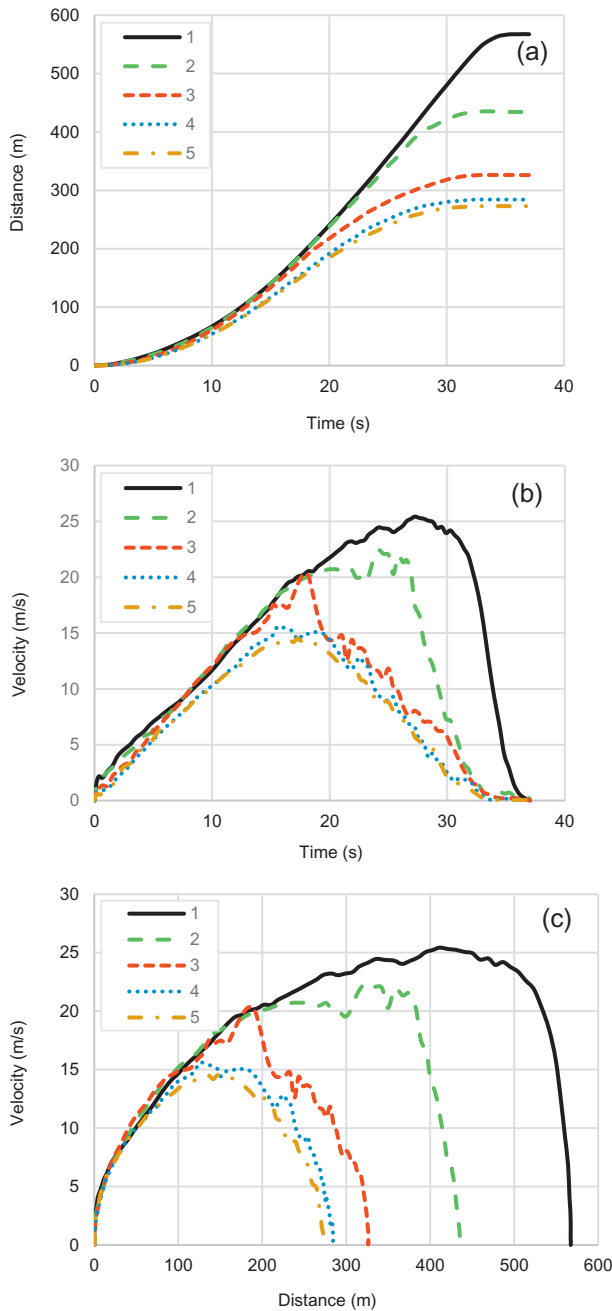


Fig. 11. Results of DDA simulations for section VII at the degraded state for the longitudinal profile: a) Distance/Time; b) Velocity/Time; c) Velocity/Distance (See Fig. 9 for history point location).

c) Degraded state

Finally, we applied the proposed bi-linear friction law in section VII with 25% friction degradation in both the clay base and rock mass (Fig. 10). The friction coefficient in the basal plane degraded therefore to a minimum value of $\mu = 0.158$. In the simulations performed under these conditions we tracked the output of both the longitudinal and vertical measurement point profiles (see Fig. 9) and also varied the joint spacing to study block size effect.

4. Results

4.1. Effects of friction degradation

The output of longitudinal measurement points 1–5 in section VII at

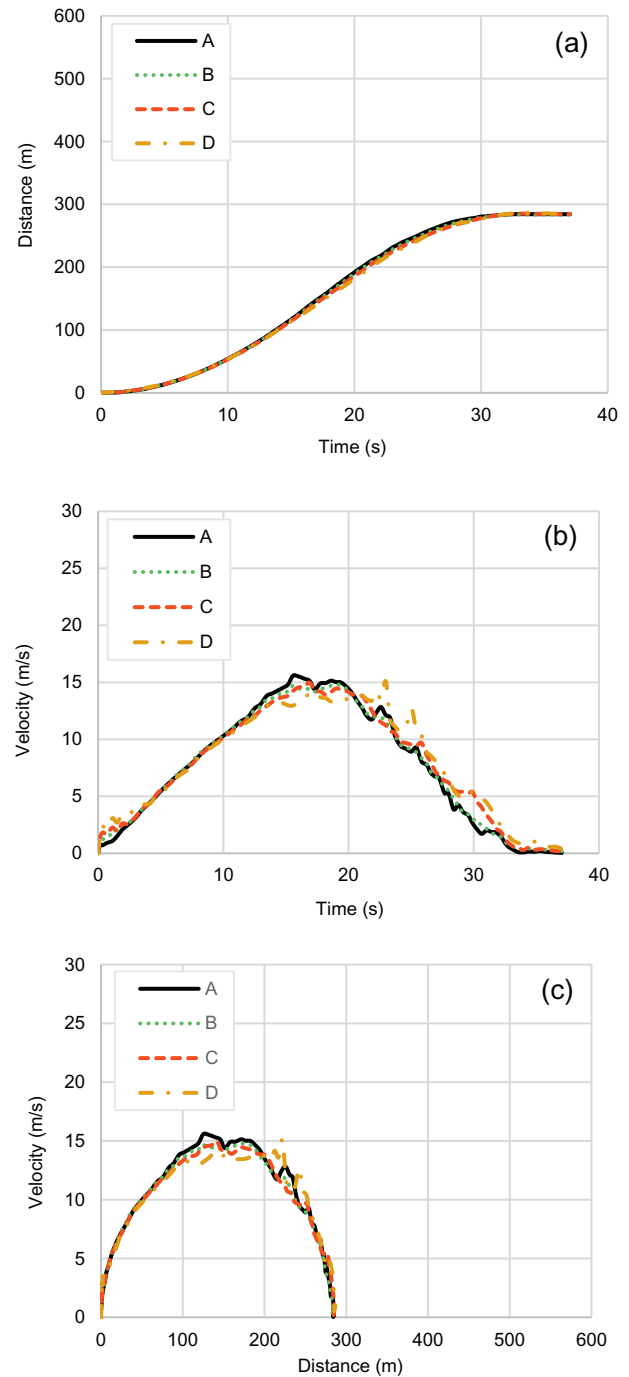


Fig. 12. Results of DDA simulations for section VII at the degraded state for the vertical profile: a) Distance/Time; b) Velocity/Time; c) Velocity/Distance (See Fig. 9 for history point location).

the degraded state are plotted in Fig. 11 and the output of the vertical measurement points A – D are plotted in Fig. 12 in displacement, velocity, and acceleration vs. time space. The final configuration of the sliding mass is shown in Fig. 13 where the lateral displacement for each measurement point can be depicted. The numerically obtained maximum displacement and peak velocities are provided in Table 3. The velocity – distance relationship for point 1 are compared with the analytical estimation (Hendron and Patton, 1985) in Fig. 14.

The complete displacement history is best appreciated from inspection of the output of measurement point 1; the motion of the other measurement points in the longitudinal direction (1–4) is arrested by piling up of blocks in the valley and across the opposite bank (see

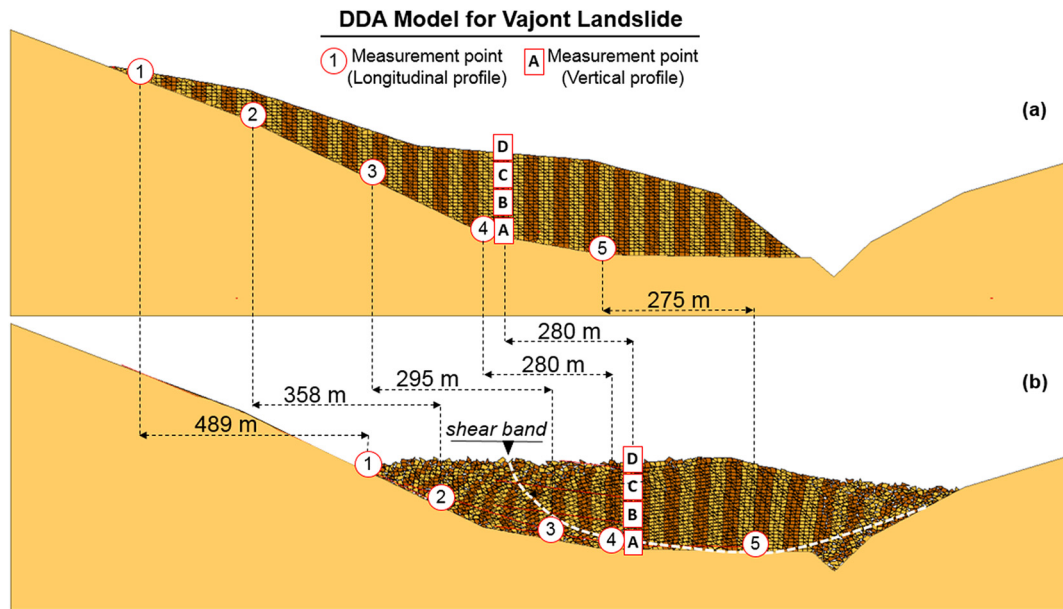


Fig. 13. Original (a) and final (b) configuration of the sliding mass as simulated with DDA at the degraded state of section VII.

Table 3

Maximum displacement and peak velocity data for section VII at the degraded state as obtained with DDA.

| Measurement Point | Maximum distance (m) | | Peak velocity (m/s) | | Time (s) |
|-------------------|----------------------|-------|---------------------|-------|----------|
| | Lateral | Total | Lateral | Total | |
| 1 | 489 | 567 | 22.0 | 25.2 | 37 |
| 2 | 358 | 434 | 20.5 | 22.4 | 35 |
| 3 | 295 | 326 | 20.9 | 22.0 | 34 |
| 4 | 280 | 285 | 15.1 | 15.4 | 33 |
| 5 | 275 | 273 | 13.9 | 14.3 | 33 |
| A | 279 | 285 | 15.0 | 15.5 | 33 |
| B | 280 | 285 | 14.8 | 15.0 | 33 |
| C | 280 | 285 | 14.7 | 15.0 | 33 |
| D | 281 | 285 | 14.2 | 14.5 | 33 |

case of Vajont landslide. DDA Sections I – X (Table 2) are computed with DDA under degraded shear strength conditions to analyze the effect of block size on distance – velocity relationship (Figs. 15 and 16) with the top of the slide (point 1) used for reference. Our results are compared with the analytical estimate of Hendron and Patton (1985) and with DDA results obtained by Sitar et al. (2005) for coarser block systems consisting of 105 and 28 blocks (a third model with only 12 blocks was not compared). As originally suggested by Sitar et al. (2005), the sliding mass indeed accelerates with increasing number of blocks, but this size effect appears to be much stronger than previously assumed. Sitar et al. (2005) suggested that internal disintegration of the sliding mass prompted increased velocities, namely sliding accelerated due to disintegration of the sliding mass. Our results confirm that sliding accelerates with decreasing block size (or with increasing number of blocks) but because our shear strength degradation is scale dependent, with maximum degradation achieved after the displacement distance equals to 1% of the overriding block length, the smaller the block size, the smaller is the displacement required to reach residual conditions.

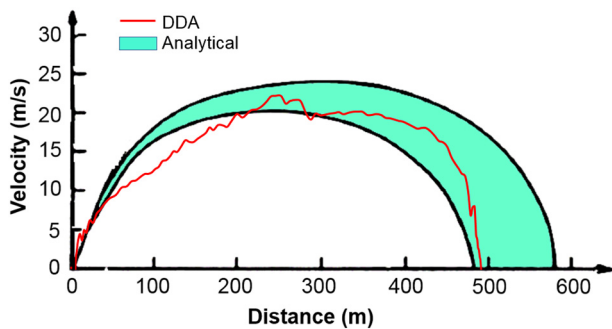


Fig. 14. Comparison between numerical (DDA) and analytical (Hendron and Patton, 1985) velocity/displacement evolution in section VII at the degraded state (point 1 used for reference).

Fig. 13). Inspection of the output of the vertical profile, however, (points A – D) confirms that the slide moved coherently, as originally suggested by Sitar et al. (2005).

4.2. Block size effect

It has been proposed that average block size affects velocity and distance results and also can affect the failure mechanism (e.g. Hencher et al., 1996). Here we study the validity of this assumption using the

5. Discussion

5.1. Deformation of sliding mass

The layout of the deformed rock mass after sliding in Section 5 (Hendron and Patton, 1985) is shown in Fig. 13b (see also Fig. 1b). Snapshots of the slide evolution as computed with DDA are shown in Fig. 17 with spatial velocity evolution. It is evident that DDA simulations are in excellent agreement with field mapping results.

This agreement includes the geometry of deformed and sheared rock mass as well as the formation of failure surfaces within the sliding rock mass above the basal plane (Fig. 13b). We believe the formation of these inner-surfaces corresponds to shear bands produced during sliding due to the adjustment of the rock mass to the irregularities of base geometry. Around these surfaces the shear strains are concentrated, and over these regions, the rock mass slipped in a rigid-body-like manner, maintaining its internal coherence.

The spatial distribution of the velocity as shown in Fig. 17 provides insight to the kinematics of the landslide. At onset of sliding (Fig. 17a) velocity zonation is formed between the top, body and toe of the slide. The toe area, not included in the longitudinal profile, is strongly

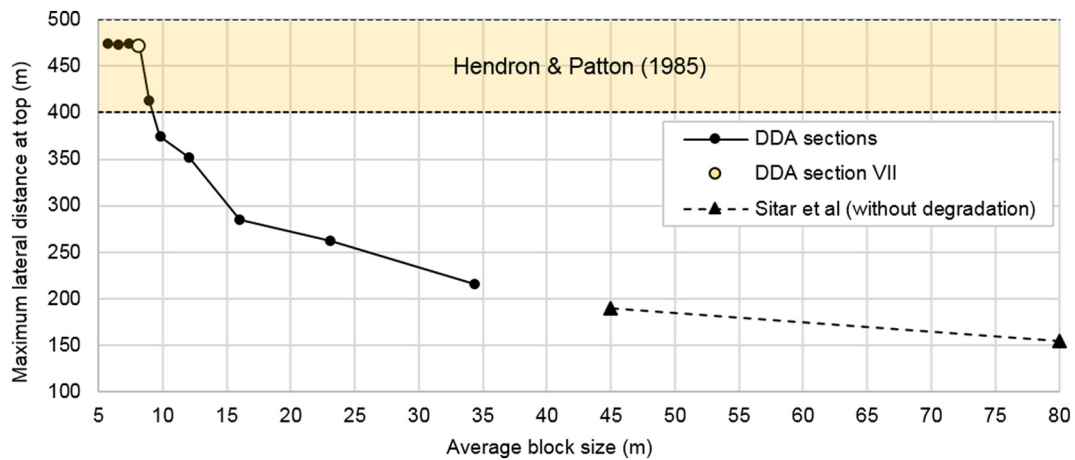


Fig. 15. Block size effect on maximum sliding distance as obtained with DDA for section VII. Analytical estimate (Hendron and Patton, 1985) and DDA results with fewer number of blocks (Sitar et al., 2005) are shown for comparison.

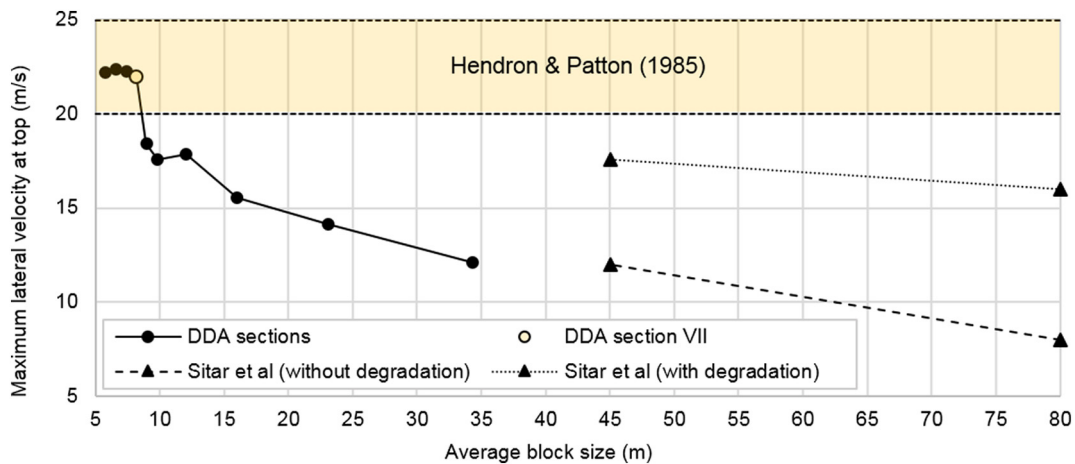


Fig. 16. Block size effect on maximum sliding velocity as obtained with DDA for section VII. Analytical estimate (Hendron and Patton, 1985) and DDA results with fewer number of blocks with and without shear strength degradation (Sitar et al., 2005) are shown for comparison.

affected by the valley trough (Fig. 17b, c). It undergoes high velocities at the beginning of the sliding and exhibits a chaotic displacement pattern because of the valley trough. The central body moves like a rigid coherent body without the effect of valley trough that is already filled with debris (Fig. 17c, d). The top area moves at the highest velocities (Fig. 17c) and to the longest distances as it slips down the relatively steeply inclined segment of the sliding surface (slope 2 in see Fig. 9). After 20 s the top begins to thicken and energy is dissipating as the slide center deaccelerates (Fig. 17d, e) at the transition between slope segments 2 and 3 (see Fig. 9). The pronounced 20° decrease in slope inclination generates both kinematic adjustment and shear band formations in the slide mass.

5.2. Comparing between DDA and LEA results

A comparison between modified DDA results and analytical limit equilibrium analysis is shown in Fig. 14. The DDA solution corresponding to the degraded state (25% friction degradation in both the basal plane and rock joints) is supported by the mapped runout distance in the field. It is comparable to the 50% degradation condition in the analytical model used by Hendron and Patton (1985) and we consider this as the best fit solution of the back analysis of the landslide.

5.3. Block size effect

Results shown in Figs. 15 and 16 clearly indicate that the number of

modeled blocks strongly influences the kinematics of sliding. The smaller the block size the higher the displacement and velocities achieved during the sliding event. This trend was also observed by Sitar et al. (2005) who have suggested that slide mass disintegration prompts acceleration. While we accept this conclusion, we explain this by the degradation model proposed here that is in fact scale dependent. If after displacement magnitude of 1% of the block length the surface slides under residual conditions, then it is to be expected that both velocity and runout distance will increase with decreasing block size. Our analysis with as many as 6255 blocks (model X) shows how dramatic this effect actually is. Regarding the Vajont case specifically, we find that the best match with field observations is obtained with a mean block size of 8 m.

6. Implications to shear heating and friction degradation

The issue of rapid shear, consequent shear heating, and how these processes affect friction degradation has been a subject of intense research over the past decade, when it became apparent that seismic velocities may reach values approaching 1 m/s. Di Toro et al. (2004) showed, using rotary shear, that friction coefficient of quartz rocks drops to values near 0.2 at shear velocity of 0.1 m/s. They proposed that by extrapolation, friction will drop to zero when the sliding velocity will approach 1 m/s. Goldsby and Tullis (2011), using continuously varying-velocity (CVV) tests, were able to apply shear velocities of up to 0.4 m/s on several different crystalline rocks and found that the friction

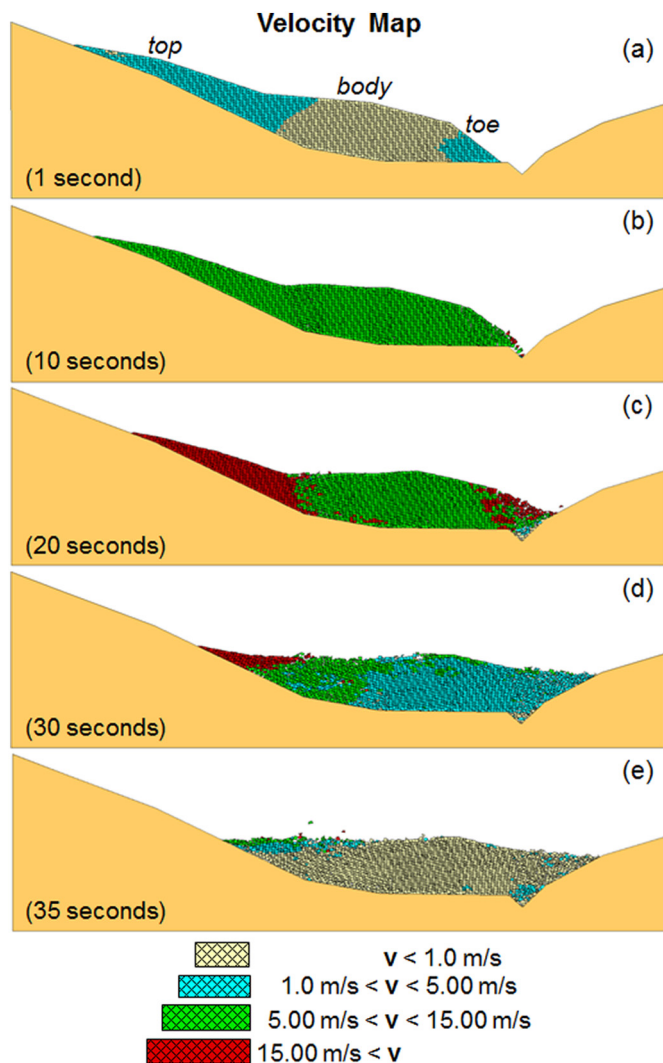


Fig. 17. DDA degraded state in section VII: Velocity color map for a) 1 s; b) 10 s, c) 20 s, d) 30 s, e) 35 s.

coefficient dropped below 0.2 at the highest velocity they achieved experimentally. They referred to the governing mechanical process as “flash” heating of microscopic asperity contacts resulting in degradation of their shear strength. Di Toro et al. (2011) present data from more than 300 rotary shear tests at slip rates between 0.1 and 2.6 m/s reporting a significant decrease in friction coefficient both for cohesive as well as non-cohesive rocks, in a process they called “fault lubrication”, to values approaching 0.1 at velocities approaching 1 m/s.

The tests reviewed above were limited in the distance of shearing to several meters at the most. Kitajima et al. (2010) tested fault gouge layer using rotary shear and were able to shear at velocities of 0.1–1.3 m/s to displacements of up to 84 m. They were able to distinguish between four distinct gouge units that form during the deformation, and showed that when heat generation was sufficiently high the coefficient dropped to 0.2. Reches and Lockner (2010) also studied gouge material in rotary shear and suggested that the formation of powder “lubrication” leads to a nonlinear trend in friction degradation. They argued that at modest slip velocities of 10–60 mm/s newly formed gouge organized into a thin deforming layer that reduced the discontinuity strength by a factor of 2–3. After slip, the gouge rapidly ‘aged’ and the surface regained its strength in a matter of hours to days.

In a recent publication (Chen et al., 2017) the same group defines three stages of strength evolution using a rotary shear apparatus at moderate slip velocities of 0.01–0.11 m/s, normal stress of 1.0–6.8 MPa,

and slip distance of up to 60 m. In Stage I, the sheared interface exhibits initial weakening in which the friction coefficient drops to a steady state level of $\mu \approx 0.3$. This weakening is associated with powder lubrication and the development of cohesive gouge layers. Stage II includes strengthening to $\mu \approx 0.5$ associated with volumetric expansion, melting of fault patches, and viscous braking at these patches. In Stage III, fault weakening is due to melt lubrication when the melted patches reach a critical fraction of the fault surface area. They show that the complex weakening-strengthening-weakening evolution is controlled by thermally activated deformation processes.

For describing the triggering process of the Tsaoling rock avalanche in Taiwan, Wu et al. (2017) developed a new dynamic ring-shear test with a maximum normal stress higher than 3.4 MPa. They conducted both static and dynamic tests on a wet sliding surface between sandstone and consolidated remolded shale. They reported residual friction values for the Tsaoling rock avalanche basal plane as low as $\mu \approx 0.10$.

These laboratory experiments shed light on dynamic mechanisms associated with rapid slip across rock discontinuities. They provide a framework for discussion of the implications of the results of the back analysis of the Vajont failure with the modified version of DDA that includes friction degradation. First, We obtain convincing evidence from the field that the friction coefficient can indeed drop below 0.2 when velocities exceed 1 m/s (Kitajima et al., 2010; Di Toro et al., 2011; Goldsby and Tullis, 2011). Moreover, We obtain a rationale for the shear strength recovery the sliding surface has experienced between historic sliding episodes and the final catastrophic failure (Reches and Lockner, 2010; Chen et al., 2017) as it would be reasonable to assume that sheared patches across the basal plane healed over time. But the most important conclusion that can be derived from the back analysis of the slide, is that in contrast to previous assumptions (Di Toro et al., 2004), the friction coefficient never drops to zero, even when the sliding velocity is greater than 10 m/s, and when the sliding distance is greater than 100 m. One may argue that perhaps the presence of water in the sliding interface could induce friction degradation to zero by vaporization, but we have every reason to believe that sliding in Vajont occurred under saturated conditions, and therefore vaporization, if occurred, did not suppress shear resistance so much.

Finally, it may be concluded that shear degradation does approach some asymptotic low boundary which for the materials studied here, namely clay filled dolomite interfaces, is determined to be at $\mu \approx 0.16$. This conclusion is in agreement with extensive test data presented by Song et al. (2016) where materials from the sliding surface of the Dagangbao landslide were tested in rotary shear at sliding velocities of 0.05 m/s to 1.3 m/s and displacements of up to 50 m. Their results clearly show an ultimate friction coefficient degradation down to $\mu \approx 0.155$ –0.158. The tests were performed under normal stress of 11.47 MPa for dolomite interfaces, and 2 MPa for gouge material from the sliding surface. The normal stress acting on the basal plane in the case of the Vajont slide can be estimated from the thickness of the sliding mass, and could not have been much greater than 6 MPa, well within the tested range in the comprehensive data set presented by Song et al. (2016).

7. Conclusions

We implement a simple bi-linear friction degradation law into DDA to model the deformation of the Vajont landslide with emphasis on sliding velocity, runoff distance, and event duration. We obtain the results that correspond the landslide final configuration by applying 25% degradation to the assumed friction of the basal plane before the catastrophic failure initiated, and 25% degradation to the assumed friction of the rock joints in the sliding mass. The duration of the event was 37 s. We find that the top of the landslide experienced the highest velocity (22 m/s peak lateral velocity) and highest runoff distance (489 m lateral displacement). These results are in agreement with values reported by Hendron and Patton (1985) for 50% friction

degradation in the basal plane using limit equilibrium analysis. The body of the sliding mass experienced lower peak velocities (15 m/s) and runout distances (280 m). This bimodal kinematical behavior is related to the flattening of the angle of the sliding plane. We find that the number of blocks in the sliding mass has very important effect on the results, in agreement with an earlier study (Sitar et al., 2005) that suggested that the disintegration of the sliding mass to many blocks prompted further slide accelerations. We believe our back analysis of the slide, that for the first time includes a detailed mesh consisting of thousands of blocks and an enhanced forward modeling code that incorporates friction degradation as a function of displacement, provides field-scale shear strength values that can constrain assumptions regarding velocity – friction relationships that are primarily based on rotary shear experiments. It is very difficult to reach velocities and distances such as modeled here in laboratory experiments, that are typically limited to velocities of up to 1 m/s and slip distances of tens of meters at the most. Using results of our back analysis we can confirm the observed tendency of the friction coefficient to drop to below 0.2 when the sliding velocity approaches 1 m/s. Moreover, we find that the degradation of the friction coefficient stops at a certain value, which for the dolomite interfaces with clay infilling studied here is found to be at $\mu \approx 0.16$.

References

- Alonso, E.E., Pinyol, N.M., 2010. Criteria for rapid sliding I A review of Vaiont case. *Eng. Geol.* 114, 198–210.
- Badt, N., Hatzor, Y.H., Toussaint, R., Sagy, A., 2016. Geometrical evolution of interlocked rough slip surfaces: the role of normal stress. *Earth Planet. Sci. Lett.* 443, 153–161.
- Bakun-Mazor, D., Hatzor, Y.H., Glaser, S.D., 2012. Dynamic sliding of tetrahedral wedge: the role of interface friction. *Int. J. Numer. Anal. Met.* 36, 327–343.
- Bandis, S., Lumsden, A.C., Barton, N.R., 1981. Experimental studies of scale effects on the shear behaviour of rock joints. *Int. J. Rock Mech. Mining Sci. Geomech.* 18, 1–21.
- Barla, G., Paronuzzi, P., 2013. The 1963 Vajont landslide: 50th anniversary. *Rock Mech. Rock Eng.* 46, 1267–1270.
- Barton, N., 1973. Review of a new shear-strength criterion for rock joints. *Eng. Geol.* 7, 287–332.
- Barton, N., Bandis, S., 1980. Some effects of scale on the shear strength of joints. *Int. J. Rock Mech. Mining Sci. Geomech.* 17 (1), 69–73.
- Barton, N., Choubey, V., 1977. The shear strength of rock joints in theory and practice. *Rock Mech.* 10, 1–54.
- Chen, X.F., Madden, A.S.E., Reches, Z., 2017. The frictional strength of talc gouge in high-velocity shear experiments. *J. Geophys. Res. Solid Earth* 122, 3661–3676.
- Chowdhury, R., 1978. Analysis of the Vajont slide - new approach. *Rock Mech. J. Int. Soc. Rock Mech.* 11, 29–38.
- Davidesko, G., Sagy, A., Hatzor, Y.H., 2014. Evolution of slip surface roughness through shear. *Geophys. Res. Lett.* 41, 1492–1498.
- Del Ventisette, C., Gigli, G., Bonini, M., Corti, G., Montanari, D., Santoro, S., Sani, F., Fantì, R., Casagli, N., 2015. Insights from analogue modelling into the deformation mechanism of the Vaiont landslide. *Geomorphology* 228, 52–59.
- Di Toro, G., Goldsby, D.L., Tullis, T.E., 2004. Friction falls towards zero in quartz rock as slip velocity approaches seismic rates. *Nature* 427, 436–439.
- Di Toro, G., Han, R., Hirose, T., De Paola, N., Nielsen, S., Mizoguchi, K., Ferri, F., Cocco, M., Shimamoto, T., 2011. Fault lubrication during earthquakes. *Nature* 471, 494 (+).
- Dieterich, J.H., 1972. Time-dependent friction in rocks. *J. Geophys. Res.* 77, 3690–3697.
- Eberhardt, E., Stead, D., Coggan, J.S., 2004. Numerical analysis of initiation and progressive failure in natural rock slopes - the 1991 Randa rockslide. *Int. J. Rock Mech. Min. Sci.* 41, 69–87.
- Giudici, F., Semenza, E., 1960. Studio geologico sul serbatoio del Vajont. In: Unpublished Report for SADE, Part a: Text, Part B: Photos with Discussions, (Venezia, Italy).
- Goldsby, D.L., Tullis, T.E., 2011. Flash heating leads to low frictional strength of crustal rocks at earthquake slip rates. *Science* 334, 216–218.
- Goren, L., Aharonov, E., 2007. Long runout landslides: the role of frictional heating and hydraulic diffusivity. *Geophys. Res. Lett.* 34.
- Goren, L., Aharonov, E., 2009. On the stability of landslides: a thermo-poro-elastic approach. *Earth Planet. Sci. Lett.* 277, 365–372.
- Habib, P., 1975. Production of gaseous pore pressure during rock slides. *J. Int. Soc.* 7, 193–197.
- Hatzor, Y.H., Ma, G., Shi, G., 2017. *Discontinuous Deformation Analysis in Rock Mechanics Practice*. CRC Press/Feng., X.T. ISRM Book Series, The Netherlands.
- Hencher, S.R., Liao, Q.H., Monaghan, B.G., 1996. Modelling slope behaviour for open-pits (vol 105, pg A37, 1996). In: *Transactions of the Institution of Mining and Metallurgy Section Mining Industry*. 105, pp. A136.
- Hendron, A.J., Patton, F.D., 1985. The Vaiont slide, a geotechnical analysis based on new geologic observations of the failure surface. In: *Technical Report GL-85-5*. Department of the Army, US Corps of Engineers, Washington, DC.
- Hendron, A.J., Patton, F.D., 1987. The Vaiont slide - a geotechnical analysis based on new geologic observations of the failure surface. *Eng. Geol.* 24, 475–491.
- Huang, D., Song, Y.X., Cen, D.F., Fu, G.Y., 2016. Numerical modeling of earthquake-induced landslide using an improved discontinuous deformation analysis considering dynamic friction degradation of joints. *Rock Mech. Rock. Eng.* 49, 4767–4786.
- Hutchinson, J.N., 1987. Mechanism producing large displacements in landslides on preexisting shears. In: *1st Sino-British Geol. Conf. Memoir of the Geological Survey of China*, pp. 175–200 Taipei.
- Hutchinson, J.N., 1988. General report: morphological and geotechnical parameters of landslides in relation to geology and hydrogeology. In: *Bonnard, C. (Ed.), Proc. 5th Int. Symp. on Landslides*, pp. 3–36 Lausanne.
- Kamai, R., Hatzor, Y.H., 2008. Numerical analysis of block stone displacements in ancient masonry structures: a new method to estimate historic ground motions. *Int. J. Numer. Anal. Met.* 32, 1321–1340.
- Kitajima, H., Chester, J.S., Chester, F.M., Shimamoto, T., 2010. High-speed friction of disaggregated ultracataclasite in rotary shear: characterization of frictional heating, mechanical behavior, and microstructure evolution. *J. Geophys. Res. Solid Earth* 115, 21.
- Lo, K.Y., Lee, C.F., Gelinis, P., 1972. Alternative interpretation of the vaiont slide. In: *Cording, E.J. (Ed.), Stability of Rock Slopes: Proc. 13th Symposium on Rock Mechanics*. ASCE, New York, Univ. Illinois, Urbana, pp. 595–623.
- Ma, S.Q., Zhao, Z.Y., Nie, W., Nemcik, J., Zhang, Z.Y., Zhu, X., 2017. Implementation of displacement-dependent Barton-Bandis rock joint model into discontinuous deformation analysis. *Comput. Geotech.* 86, 1–8.
- MacLaughlin, M., Sitar, N., Doolin, D., Abbot, T., 2001. Investigation of slope-stability kinematics using discontinuous deformation analysis. *Int. J. Rock Mech. Min.* 38, 753–762.
- Mizoguchi, K., Hirose, T., Shimamoto, T., Fukuyama, E., 2007. Reconstruction of seismic faulting by high-velocity friction experiments: an example of the 1995 Kobe earthquake. *Geophys. Res. Lett.* 34.
- Müller, L., 1964. The rock slide in the Vajont valley. *Rock Mech. Eng. Geol.* 2, 148–212.
- Müller, L., 1968. New considerations in the Vaiont slide. *Engl. J.* 6, 1–91.
- Ning, Y., Zhao, Z., 2012. A detailed investigation of block dynamic sliding by the discontinuous deformation analysis. *Int. J. Numer. Anal. Methods Geomech.* 37, 2373–2393.
- Nonveiller, E., 1986. Vaiont slide — influence of frictional heat on slip velocity. In: *Semenza, E., Melidoro, F. (Eds.), Atti del Convegno Sulla Frana del Vaiont*, pp. 493–512.
- Paronuzzi, P., Bolla, A., 2015. Gravity-induced rock mass damage related to large en masse rockslides: evidence from Vajont. *Geomorphology* 234, 28–53.
- Patton, F.D., 1966. Multiple modes of shear failure in rock. In: *Proc. 1st Congr. Int. Soc. Rock Mech. ISRM, Lisbon*, pp. 509–513.
- Pinyol, N.M., Alonso, E.E., 2010. Criteria for rapid sliding II Thermo-hydro-mechanical and scale effects in Vaiont case. *Eng. Geol.* 114, 211–227.
- Reches, Z., Lockner, D.A., 2010. Fault weakening and earthquake instability by powder lubrication. *Nature* 467 (452-U102).
- Rengers, N., 1970. Influence of surface roughness on the friction properties of rock planes. In: *Proceedings 2nd congress ISRM*, pp. 1–31 Beograd.
- Romero, S.U., Molina, R., 1974. Kinematic aspects of the Vaiont Slide. In: *Proceedings of the 3rd Congress ISRM*, pp. 865–870 Denver, Colorado.
- Ruina, A., 1983. Slip instability and state variable friction laws. *J. Geophys. Res.* 88, 10,359–10,370.
- Semenza, E., 2001. La storia del Vaiont raccontata dal geologo che ha scoperto la frana. In: *Tecomproject Editore Multimediale*, pp. 138 Ferrara, Italy.
- Semenza, E., Ghirotti, M., 2000. History of the 1963 Vaiont slide: the importance of geological factors. *Bull. Eng. Geol. Environ.* 59, 87–97.
- Shi, G.H., 1993. Block system modeling by discontinuous deformation analysis. In: *Brebbia, C.A., Connor, J.J. (Eds.), Topics in Engineering Southampton, UK*. Computational Mechanics Publication.
- Shi, G.H., 2010. *User's Manuals of Discontinuous Deformation Analysis Codes*. DDA Company, Belmont, CA.
- Sitar, N., MacLaughlin, M.M., Doolin, D.M., 2005. Influence of kinematics on landslide mobility and failure mode. *J. Geotech. Geoenviron.* 131, 716–728.
- Song, Y.X., Huang, D., Cen, D.F., 2016. Numerical modelling of the 2008 Wenchuan earthquake-triggered Daguangbao landslide using a velocity and displacement dependent friction law. *Eng. Geol.* 215, 50–68.
- Superchi, L., Floris, M., Ghirotti, M., Genevois, R., Jaboyedoff, M., Stead, D., 2010. Technical note: implementation of a geodatabase of published and unpublished data on the catastrophic Vaiont landslide. *Nat. Hazards Earth Syst. Sci.* 10, 865–873.
- Tika, T.E., Hutchinson, J.N., 1999. Ring shear tests on soil from the Vaiont landslide slip surface. *Geotechnique* 49, 59–74.
- Togo, T., Ma, S.L., Hirose, T., 2009. High-velocity friction of faults: a review and implication for landslide studies. In: *The Next Generation of Research on Earthquake-induced Landslides: an International Conference in Commemoration of 10th Anniversary of the Chi-Chi Earthquake*, pp. 205–216.
- Tsesarsky, M., Hatzor, Y.H., Sitar, N., 2005. Dynamic displacement of a block on an inclined plane: analytical, experimental and DDA results. *Rock Mech. Rock. Eng.* 38, 153–167.
- Vardoulakis, I., 2000. Catastrophic landslides due to frictional heating of the failure plane. *Mech. Cohesive-Frictional Mater.* 5, 443–467.
- Veveakis, E., Vardoulakis, I., Di Toro, G., 2007. Thermoporoelasticity of creeping landslides: the 1963 Vaiont slide, northern Italy. *J. Geophys. Res.-Earth* 112.
- Voight, B., Faust, C., 1982. Frictional heat and strength loss in some rapid landslides. *Geotechnique* 32, 43–54.
- Wang, L.-Z., Jiang, H.-Y., Yang, Z.-X., Xu, Y.-C., Zhu, X.-B., 2013. Development of discontinuous deformation analysis with displacement-dependent interface shear strength. *Comput. Geotech.* 47, 91–101.
- Wolter, A., Stead, D., Ward, B.C., Clague, J.J., Ghirotti, M., 2016. Engineering geomorphological characterisation of the Vajont slide, Italy, and a new interpretation of the chronology and evolution of the landslide. *Landslides* 13, 1067–1081.
- Wu, J.H., Liao, C.J., Lin, H.M., Fang, T.T., 2017. An experimental study to characterize the initiation of the seismic-induced Tsaoing rock avalanche. *Eng. Geol.* 217, 110–121.
- Yagoda Biran, G., Hatzor, Y.H., 2016. Benchmarking the numerical discontinuous deformation analysis method. *Comput. Geotech.* 71, 30–46.